Med Biol Eng Comput (2009) 47:221–232
DOI 10.1007/s11517-008-0430-z

SPECIAL ISSUE - REVIEW

Wave intensity analysis and the development of the reservoir–wave approach

John V. Tyberg · Justin E. Davies · Zhibin Wang · William A. Whitelaw · Jacqueline A. Flewitt · Nigel G. Shrive · Darryl P. Francis · Alun D. Hughes · Kim H. Parker · Jiun-Jr Wang

Received: 7 April 2008 / Accepted: 22 December 2008 / Published online: 3 February 2009

Abstract The parameters of wave intensity analysis are calculated from incremental changes in pressure and velocity. While it is clear that forward- and backward-traveling waves induce incremental changes in pressure, not all incremental changes in pressure are due to waves; changes in pressure may also be due to changes in the volume of a compliant structure. When the left ventricular ejects blood rapidly into the aorta, aortic pressure increases, in part, because of the increase in aortic volume: aortic inflow is momentarily greater than aortic outflow. Therefore, to properly quantify the effects of forward or backward waves on arterial pressure and velocity (flow), the component of the incremental change in arterial pressure that is due only to this increase in arterial volume—and *not*, fundamentally, due to waves—first must be excluded. This component is the pressure generated by the filling and emptying of the reservoir, Otto Frank's Windkessel.

Keywords Pressure · Windkessel · Aorta · Wave intensity analysis · Frank · Reservoir · Wave

1 Introduction

Wave intensity analysis (WIA), which is computed from incremental temporal changes in pressure (P) and in

J. V. Tyberg (✉) · J.-J. Wang
Departments of Cardiac Sciences and Physiology & Pharmacology, University of Calgary, 3330 Hospital Drive NW, Calgary, AB T2N 4N1, Canada
e-mail: jtyberg@ucalgary.ca

J.-J. Wang
e-mail: jjwang@ucalgary.ca

J. E. Davies · D. P. Francis · A. D. Hughes
Imperial College Healthcare NHS Trust, International Centre for Circulatory Health, St Mary's Hospital Campus, London, UK

J. E. Davies
e-mail: justindavies@heart123.com

D. P. Francis
e-mail: d.francis@cheerful.com

A. D. Hughes
e-mail: a.hughes@imperial.ac.uk

Z. Wang
Qingdao University Medical College Hospital, 266003 Qingdao, China
e-mail: qdecholab@yahoo.com.cn

W. A. Whitelaw
Department of Medicine (Emeritus Professor), University of Calgary, 3330 Hospital Drive NW, Calgary, AB T2N 4N1, Canada
e-mail: wwhitela@ucalgary.ca

J. A. Flewitt
Stephanson Cardiovascular MR Centre, University of Calgary, 3330 Hospital Drive NW, Calgary, AB T2N 4N1, Canada
e-mail: Jacqueline.Flewitt@calgaryhealthregion.ca

N. G. Shrive
Department of Civil Engineering, University of Calgary, 2500 University Ave. NW, Calgary, AB T2N 1N4, Canada
e-mail: ngshrive@ucalgary.ca

K. H. Parker
Physiological Flow Unit, Department of Bioengineering, Imperial College, London, UK
e-mail: k.parker@ic.ac.uk

velocity (U), has proven to be a very useful tool in hemodynamics because of its ability to identify the timing and direction of wave motion (forward- or backward-traveling, respectively in or against the direction of net blood flow) and whether a wave increases or decreases pressure as it passes [i.e., whether it is a compression or a decompression wave (formerly called an expansion wave)]. After years of using WIA to study a variety of physiological problems, we ultimately concluded that reservoir pressure should be subtracted from measured aortic pressure before wave separation by WIA is performed because not all the change in aortic pressure can be properly attributed to forward or backward wave motion. In part, aortic pressure also changes because of changes in aortic volume and this non-wave-related pressure should be discounted before WIA proceeds.

As described in detail in the preceding paper by Parker [14], WIA began with the calculation of net wave intensity (initially symbolized by $\Delta P \Delta U$) to characterize left ventricular (LV) ejection [16]. At the beginning of ejection when aortic pressure and blood velocity are increasing, WIA identifies a one-dimensional compression wave that accounts for the acceleration of the stroke volume in the face of an increasing pressure. Shortly after this compression wave, WIA identifies a decompression wave that develops slowly but accounts for the deceleration of the volume being ejected. Aortic flow decreases, stops and momentarily reverses due to this "braking action" of the relaxing LV [25]. The sign convention of net wave intensity (i.e., positive) indicates that both these waves are dominantly forward-traveling.

When studying more complicated physiological phenomena [20], it often became apparent that substantial forward- and backward-traveling waves were occurring simultaneously, making net wave intensity ambiguous; thus, it was desirable to separate net intensity into the individual contributions of the forward- and backward-traveling waves. This separation requires knowledge of the wave speed, which can be estimated with adequate accuracy by determining the slope of the relation between pressure and the product of density and velocity [9, 15], as well as by the foot-to-foot method by which the transit time for a wave to traverse a known distance is measured [2].

The parameters of WIA are calculated from incremental temporal changes in pressure and velocity at a specific cross-section of a vessel or chamber. While the passage of forward or backward waves clearly induces incremental changes in pressure, not all incremental changes in pressure are due to the passage of such

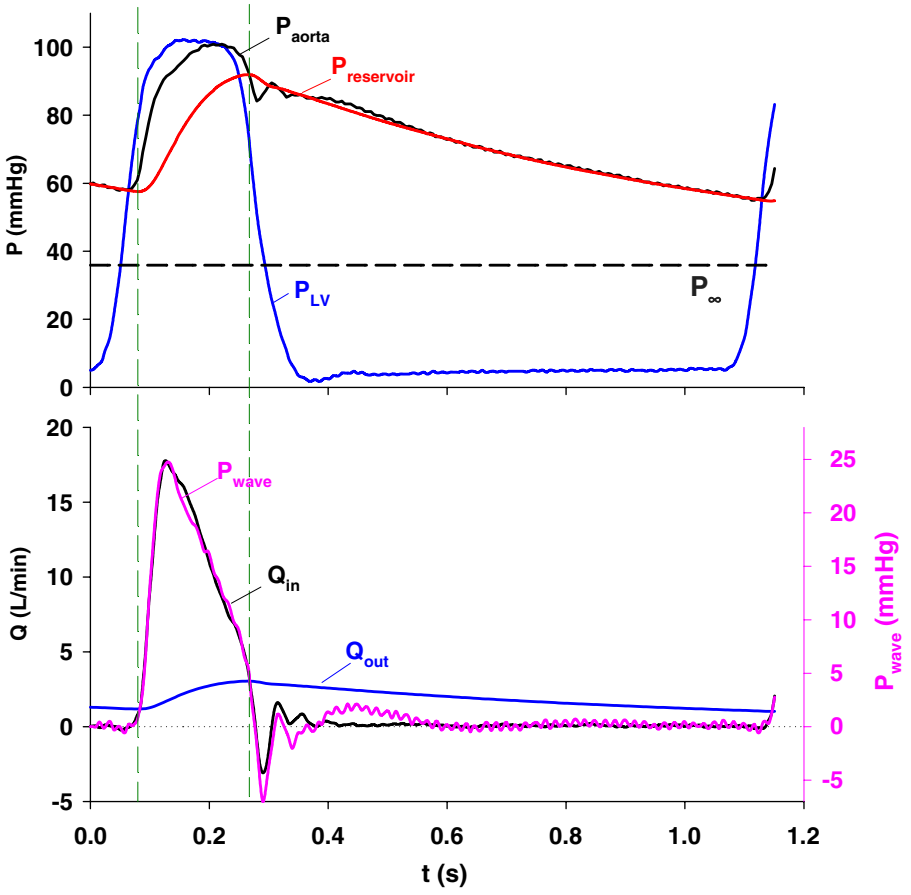

Fig. 1 The aortic Windkessel/reservoir is a hydraulic-integrator. In the *top panel* are typical aortic root pressure (P_{aorta}), left ventricular pressure (P_{LV}), calculated reservoir pressure ($P_{reservoir}$, *red line*) and the asymptotic pressure (P_{∞}, *black dashed line*). In the *lower panel* are wave-related pressure (P_{wave}, *pink line*) calculated by subtracting the reservoir pressure from the aortic pressure and aortic flow (Q_{in}, *black line*) plotted against time with the scales adjusted so that their peak values coincide. Note that they are almost identical in contour. The reservoir is charged when inflow is greater than outflow and vice versa. Two *vertical dashed lines* mark the instants when the inflow equals the outflow (Q_{out}, *blue line*), when $P_{reservoir}$ neither increases nor decreases. (Modified from Wang et al. [23] with permission of the American Physiological Society) (Color figure online)

waves—changes in pressure may also be due to the elastance/compliance of a structure. For example, during isovolumic contraction and relaxation, ventricular pressure changes because the elastance of the ventricle respectively increases or decreases, while volume nominally remains constant. During these intervals, pressure changes because of the changes of elastance and waves in the ventricle appear to be absent. In a contrasting example, when the LV ejects blood into the elastic (compliant) aorta, arterial pressure increases, in part, because aortic volume increases: aortic inflow temporarily exceeds aortic outflow [23]. Thus, when volume remains constant and elastance changes, pressure changes; when volume changes and elastance remains constant, pressure also changes. Therefore, to properly quantify the effects of forward- or backward-traveling waves on arterial pressure and velocity (flow), the component of the incremental change in arterial pressure that is due only to this increase in arterial "reservoir" volume and *not*, fundamentally, due to waves, should first be excluded. This component is the pressure associated with the reservoir—Frank's Windkessel [8, 19]. This is the rationale of separation of arterial pressure into the sum of a reservoir pressure ($P_{\text{reservoir}}$) and a wave-related pressure (P_{wave}). (In previous publications, these pressures were respectively called Windkessel pressure, after Frank [8, 19], and excess pressure, after Lighthill [10]).

2 The arterial reservoir

Because we were studying LV ejection into the aorta, we first applied the reservoir–wave principle to the aorta. To determine $P_{\text{reservoir}}$, it was observed that its rate of change ($\mathrm{d}P_{\text{reservoir}}/\mathrm{d}t$) must be proportional to its rate of change of volume, through the proportionality constant, $\mathrm{d}P/\mathrm{d}V$, which is the reciprocal of compliance (C). Since the rate of change of volume is the instantaneous difference between inflow (Q_{in}) and outflow (Q_{out}),

$$\frac{\mathrm{d}P_{\text{reservoir}}}{\mathrm{d}t} = \frac{1}{C} \times (Q_{\text{in}} - Q_{\text{out}}) \tag{1}$$

where the outflow was assumed to be driven by the gradient between $P_{\text{reservoir}}$ and the arterial asymptotic pressure (P_{∞}),

$$Q_{\text{out}} = \frac{P_{\text{reservoir}} - P_{\infty}}{R_{\text{reservoir}}} \tag{2}$$

Equation 1 becomes an ordinary equation by substituting Q_{out} using Eq. 2,

$$\frac{\mathrm{d}P_{\text{reservoir}}}{\mathrm{d}t} = \frac{Q_{\text{in}}}{C} - \frac{P_{\text{reservoir}} - P_{\infty}}{\mathrm{RC}} \tag{3}$$

There is an analytical solution for Eq. 3,

$$P_{\text{reservoir}}(t - t_0) = P_{\infty} + (P_0 - P_{\infty})\mathrm{e}^{\frac{-t}{\mathrm{RC}}} + \mathrm{e}^{\frac{-t}{\mathrm{RC}}} \int_{t_0}^{t} \frac{Q_{\text{in}}(t')}{C} \mathrm{e}^{\frac{t'}{\mathrm{RC}}} \mathrm{d}t' \tag{4}$$

In anesthetized dogs, Wang et al. [23] measured aortic pressure (P_{aorta}) and flow (Q_{in}) close to the aortic valve. Using the integral form of Eq. 1, they then iteratively solved for C, $R_{\text{reservoir}}$ and P_{∞}, where $R_{\text{reservoir}}$ is $(\overline{P_{\text{reservoir}}} - P_{\infty})$/cardiac output and P_{∞} is the pressure toward which P_{aorta} declines after infinite time.

In Eq. 4, t_0 and P_0 were the time and pressure of the first point, respectively. $Q_{\text{in}}(t)$ was the measured flow. With the knowledge of R, C and P_{∞}, Eq. 4 ($P_{\text{reservoir}}$ with respect to time) can be determined. $P_{\text{reservoir}}$ varies in magnitude, τ, etc., through changes of R, C and P_{∞}. Using a Matlab

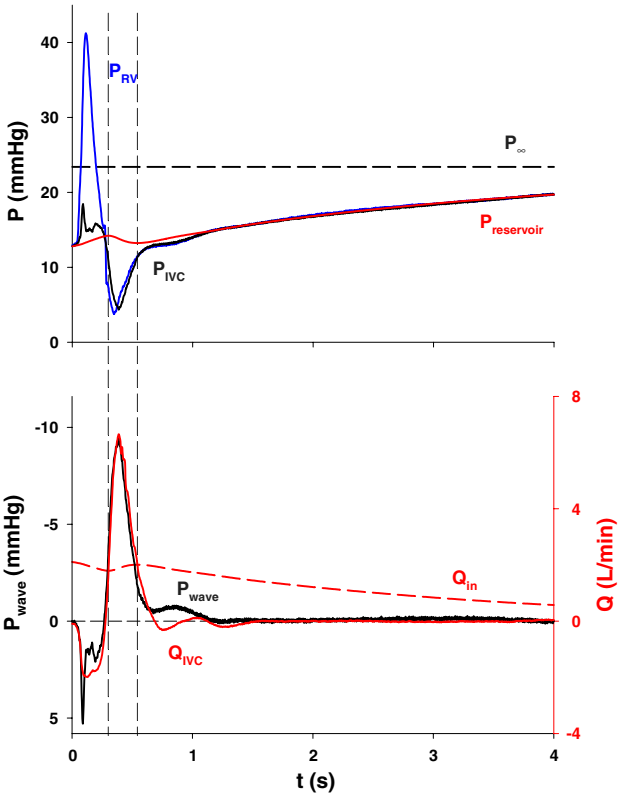

Fig. 2 The venous (*IVC* inferior vena cava) Windkessel/reservoir is also a hydraulic integrator. The *top panel* shows measured P_{RV} (*blue*) and P_{IVC} (*black*) and calculated reservoir pressure ($P_{\text{reservoir}}$, *red*) and asymptotic pressure (P_{∞}, *black dashed line*). The *bottom panel* shows measured Q_{IVC} and calculated inflow (Q_{in}). Calculated wave-related pressure (P_{wave}) is proportional to Q_{IVC}. The *vertical black dashed lines* indicate the instants at which $Q_{\text{in}} = Q_{\text{IVC}}$, when $P_{\text{reservoir}}$ neither increases nor decreases. (The long cardiac cycle was induced by an injection of acetylcholine). (Modified from Wang et al. [22] with permission of the American Physiological Society) (Color figure online)

search algorithm, the parameters were determined by minimizing the squared errors between the calculated $P_{reservoir}$ and measured P_{aorta} during late diastole, during which time we assumed that the change in pressure was due to the discharging of aortic volume. The calculated values of the parameters generally converged satisfactorily if the *R–R* interval was greater than 0.7 s. In our study, intermittent long beats (*R–R* interval, 1.5–2 s) were induced using vagal stimulation or a bolus of acetylcholine in the RA. Parameters were determined using the last long diastole and the same values were used to calculate $P_{reservoir}$ for the immediately preceding steady-state beats.

Figure 1 illustrates the results of this analysis and the hydraulic-integrator behavior of the Windkessel/reservoir. There are two instants (see the two vertical dashed lines) during the cardiac cycle when $Q_{in} = Q_{out}$: just after the beginning of ejection, when Q_{in} has increased enough to equal Q_{out}, and near the end of ejection, when Q_{in} has decreased enough to again equal Q_{out}. As dictated by Eq. 1, at those two instants $dP_{reservoir}/dt = 0$ so the $P_{reservoir}$ waveform is momentarily flat. During ejection and between the vertical lines, Q_{in} is greater than Q_{out} and $P_{reservoir}$ increases. During the remainder of the cycle, Q_{in} is less than Q_{out} and $P_{reservoir}$ decreases. In the anesthetized dog, P_{wave} is almost perfectly proportional to Q_{in}, indicating that the nearly identical, superimposed P_{wave} and Q_{in} waveforms result only from the forward-traveling compression and decompression waves generated by the LV (see lower panel of Fig. 1). (Wave reflection during systole might be more important in aged human subjects). The ratio of P_{wave} to Q_{in} is interpreted as the resistance of the proximal aorta (see Sect. 8, below).

3 The venous reservoir

The arterial reservoir, which buffers the intermittent filling due to the ejection of the LV and thus modulates arterial pressure and reservoir outflow, is not the only hydraulic integrator in the cardiovascular system. A venous reservoir buffers the intermittent emptying of the veins due to the filling of the RV, modulating venous pressure and reservoir inflow. To define the venous reservoir (Windkessel), Wang inverted the logic he had used to solve the parameters of the arterial reservoir [22]. Figure 2 demonstrates the integrating behavior of the venous reservoir, inflow being

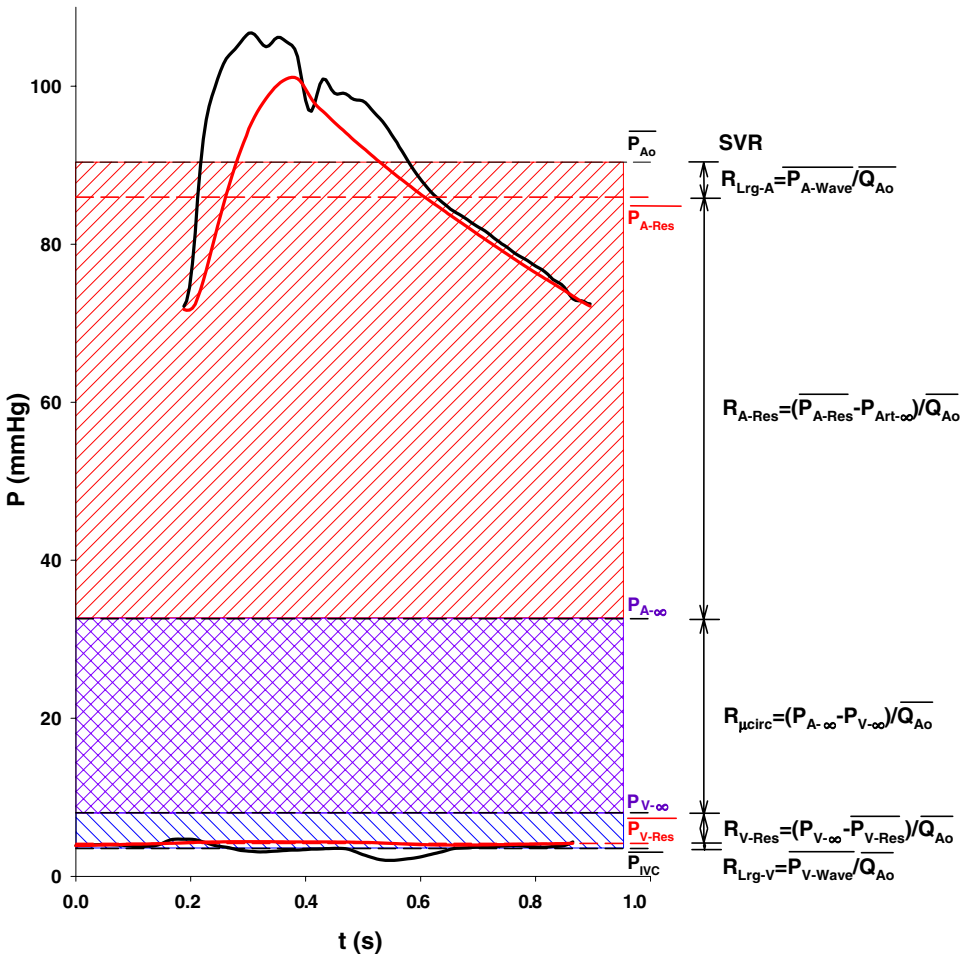

Fig. 3 Systemic resistances related to arterial and venous reservoirs. *Upper and lower black curves* indicate simultaneously measured arterial and IVC pressures and *upper and lower red curves*, their calculated reservoir pressures. The mean values of aortic $(\overline{P_{Ao}})$, arterial reservoir (P_{A-Res}), IVC reservoir pressure $(\overline{P_{V-Res}})$ and IVC pressure $(\overline{P_{IVC}})$ are indicated by *labeled horizontal dashed lines*; also, arterial asymptotic pressure $(P_{A-\infty})$ and IVC asymptotic pressure $(P_{V-\infty})$. The total arterial–venous pressure gradient was separated into arterial (*red hatching*, related to the large arteries and the arterial reservoir), microcirculatory (*purple cross-hatching*) and venous (*blue hatching*, related to the large veins and the venous reservoir) elements (Color figure online)

equal to outflow (i.e., Q_{IVC}) near the beginning and near the end of the brief interval of rapid RV diastolic filling. During the remainder of diastole, inflow from the microcirculation continues at a decreasing rate as $P_{reservoir}$ increases, approaching (venous) P_{∞}. Once again, P_{wave} is almost perfectly proportional to Q_{IVC}, indicating that the nearly identical P_{wave} and Q_{IVC} waveforms are, for the most part, the result of the backward-traveling waves generated by the RV. Also once again, the ratio of P_{wave} to Q_{IVC} is interpreted as the resistance of the large veins (i.e., inferior vena cava) between the right atrium and the venous reservoir. (Wang et al. also calculated reservoir parameters for the superior vena cava [22]).

4 Implications of Windkessel/reservoir analysis on systemic vascular resistance

The presence of an arterial and a venous reservoir with their associated reservoir and large-artery/large-vein resistances invited a reconsideration of systemic vascular resistance as a network of individual resistances arranged in series [22] (see Fig. 3). The resistances associated with the arterial and venous reservoirs were calculated as described above and the resistance of the microcirculation was calculated by difference (it can also be calculated as the difference between arterial and venous values of P_{∞}, divided by cardiac output). When these values were compared to the results of the micro-puncture experiments of Davis et al. [6], there was good agreement (see Fig. 7 in Wang et al. [22]). The comparison suggests symmetry between the arterial and venous reservoirs in that both reservoirs seem to extend to micro-vessels as small as ~60 μm in diameter. Recently, we studied the effects of vasodilatation (sodium nitroprusside, NP) and vasoconstriction (methoxamine, Mtx) on this system and found that ~50% of the LV stroke work is normally dissipated by the arterial reservoir resistance (NP, ~36%; Mtx, ~27%) and ~20% normally by the large-artery resistance (NP, ~37%; Mtx, ~6%) [24].

Figure 3 defines the relation of the series resistances but the relation of the compliances has not been defined. Calculation of the arterial reservoir outflow and the venous reservoir inflow yields different waveforms, which implies that the microcirculation must also be characterized with a parallel capacitance. What are the relative magnitudes of the arterial, venous and microcirculatory capacitances? Figure 4 shows an analogous electrical circuit diagram that illustrates the series resistance arrangement with capacitors spanning the arterial reservoir resistance, the microcirculatory resistance and the venous reservoir resistance.

As shown in Fig. 5, the differences in the inflow and outflow (vertical left-hand panels) of the arterial, the microcirculatory and the venous sections of the circulation are

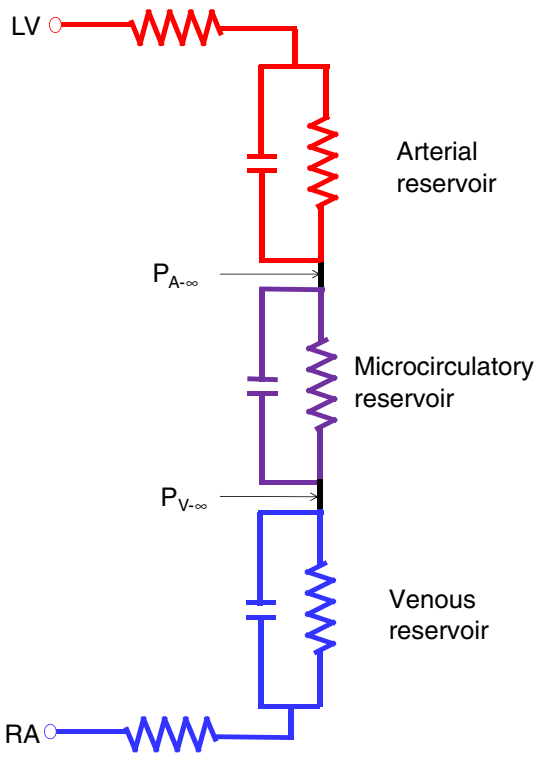

Fig. 4 An analogous electrical circuit diagram of the systemic circulation showing arterial (*red*), microcirculatory (*purple*) and venous (*blue*) elements (Color figure online)

equal to the net flows in to (positive values) and out of (negative values) the respective capacitors (vertical middle panels). Further, integration of these flow waveforms yields the change in volume of the respective capacitors during a cardiac cycle (right-hand panel). In this typical example, the change in volume of the arterial reservoir (i.e., capacitor) is equal to 16.7 mL or 85% of the stroke volume (i.e., 19.6 mL). The change in volume of the venous reservoir is 6.0 mL or 35% of that of the arterial reservoir (i.e., 30% of the stroke volume) and the change in volume of the microcirculatory reservoir is 1.5 mL or 10% of that of the arterial reservoir (i.e., 8% of the stroke volume). Thus, while measurable, the change in volume of the microcirculatory element of the systemic circulation is small compared to the arterial element, which must be large to accommodate the large difference between inflow and outflow during LV ejection.

5 Extension of Windkessel/reservoir analysis to left ventricular filling

Flewitt et al. [7] applied these principles to account for the reservoir effect in their study of the dynamics of LV filling. When they compared their results to those previously reported [24], they found that the energy of the backward

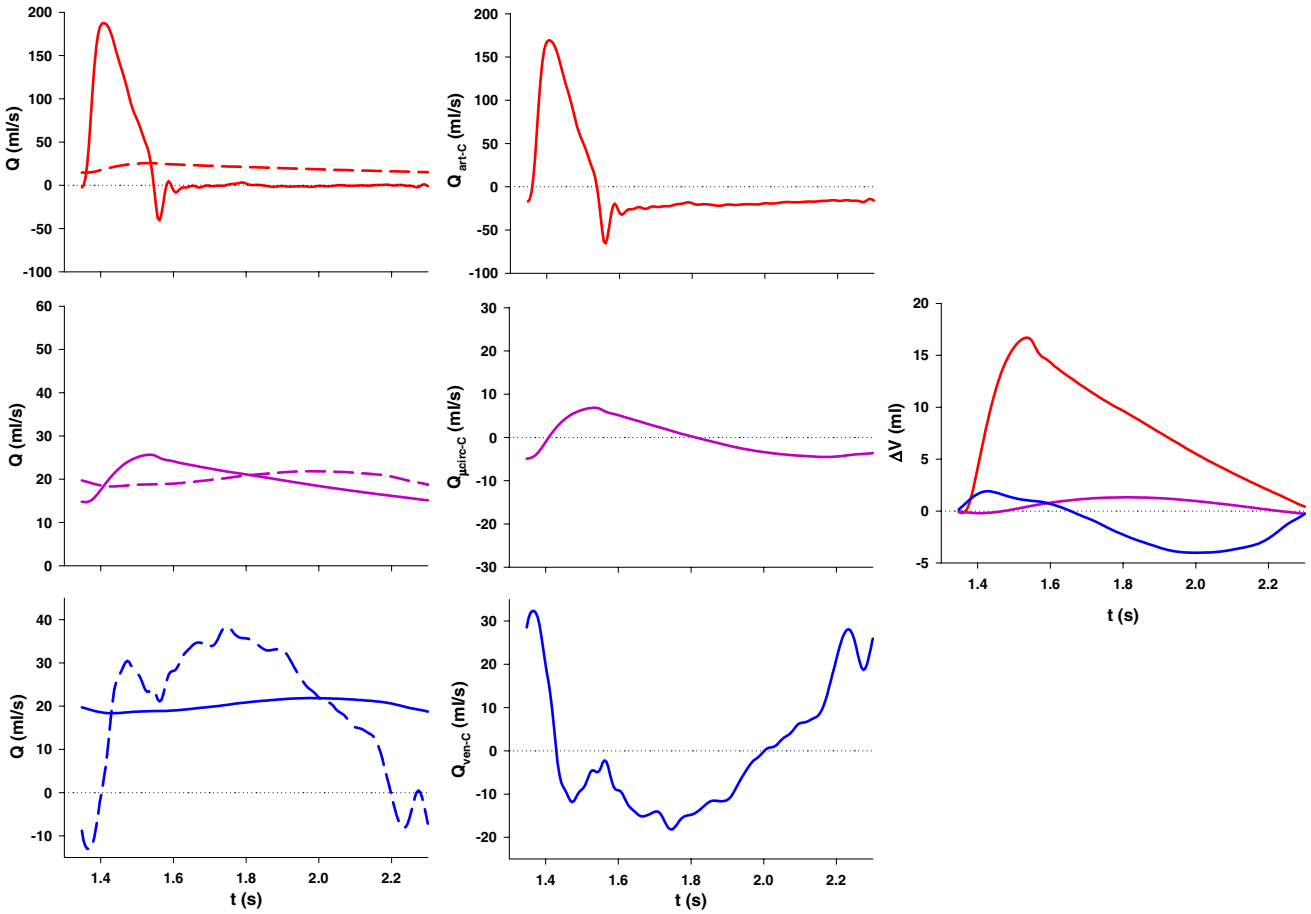

Fig. 5 A comparison of the arterial (*red*), microcirculatory (*purple*) and venous (*blue*) capacitive elements in the systemic circulation (see Fig. 4). The *vertical left-hand panels* show the respective inflows (*solid lines*) and outflows (*dashed lines*) of each of these elements. Note that the inflow of the microcirculatory element is equal to the outflow of the arterial element and that the outflow of the microcirculatory element is equal to the inflow of the venous element. The *vertical middle panels* show the respective flows in to and out of the capacitors. The *right-hand panel* shows a comparison of the volume changes accommodated by the arterial, microcirculatory and venous capacitors (reservoirs). (Note that arterial inflow and outflow (*upper panels*) are shown on a less-sensitive scale). Data from a typical example (Color figure online)

decompression wave responsible for diastolic suction was 2.6-fold greater than previously reported. The numerical correction may be of only limited interest but the extension of the principle—reservoir-related pressure changes should be discounted before analyzing wave motion—is very important.

6 Aortic wave propagation and reflection

Although it is seemingly more straightforward to calculate the parameters of the aortic reservoir at the ascending aorta, where diastolic inflow is 0, Wang's approach [23] can theoretically be applied at any point in the aorta where pressure and flow (velocity) are determined. Our preliminary results suggest a profoundly different picture of how the aortic pressure waveform at different locations in the aorta is constituted.

Figure 6 is based on simultaneous measurements of pressure and flow at the aortic root and Fig. 7, 20-cm distal, in the descending thoracic aorta of an anesthetized dog. In Fig. 6, note that there are no significant backward-traveling waves at the aortic valve. However, the measured, dome-shaped, aortic pressure is shown to be the sum of a triangular pressure waveform due to the forward-traveling waves and the reservoir pressure. The triangular flow waveform has generally been attributed to the arrival of a backward-traveling (compression) wave but the present analysis suggests that the triangular (forward) pressure and flow waveforms are simply due to the temporal pattern of LV contraction and relaxation [16]. Contraction begins and ends very quickly, generating a tall, narrow, spike-shaped dI_{W+} pattern and a rapid upstroke in (forward) pressure and flow. Relaxation begins very early during ejection but develops more gradually and does not generate a substantial forward decompression wave until just before the end of systole.

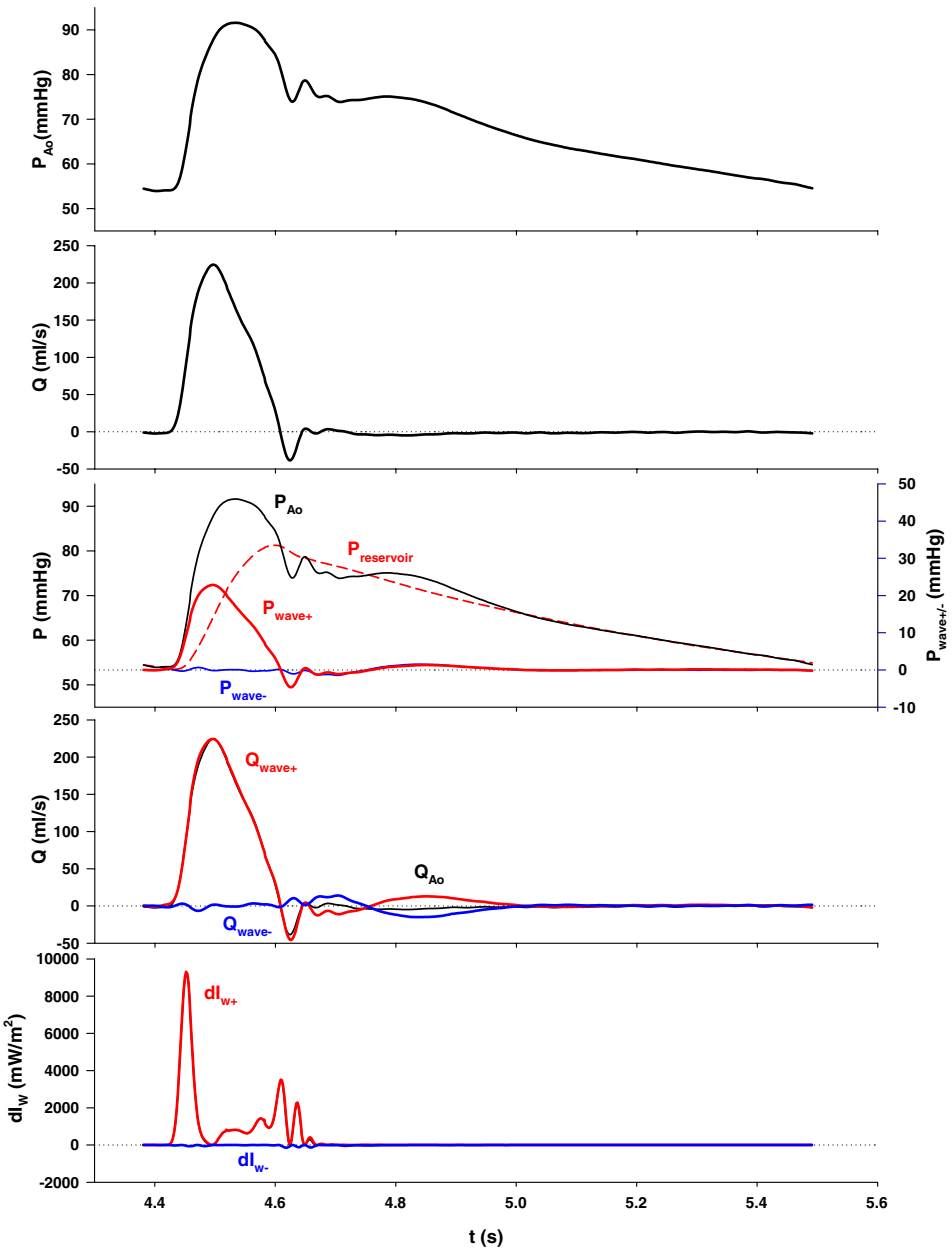

Fig. 6 Reservoir–wave analysis of data recorded from the ascending aorta in a dog. In the *top panels*, measured arterial pressure is shown; in the *next panels*, measured flow; in the *next panels*, measured pressure (again) with its components: reservoir pressure (*red dashed line*), the pressure due the passage of forward-traveling waves (*solid red line*) and the pressure due the passage of backward-traveling waves (*solid blue line*); in the *next panels*, measured flow (again) with its components: the flow due the passage of forward-traveling waves (*solid red line*), and the flow due the passage of backward-traveling waves (*solid blue line*) and finally, in the *bottom panels*, the separated wave intensity analysis. dI_{W+} (the intensity of forward-traveling waves) is shown as *positive* and in *red* and dI_{W-} (the intensity of backward-traveling waves) is shown as *negative* and in *blue*. Note that the pressure waveform due to forward-traveling waves is the same *triangular shape* as the flow waveform (Color figure online)

As WIA highlights, LV "relaxation" is a complicated process. At the beginning of ejection, the LV generates a FCW that accelerates the LV stroke volume to a peak velocity, while the opposing aortic pressure continues to increase. After that period of acceleration, in principle, the LV might have continued shortening at a rate just sufficient *to maintain the peak velocity, unchanged*, during which interval waves would have been absent [17]. However, the flow waveform in the ascending aorta is characteristically triangular such that acceleration is followed immediately by deceleration. (The timing of the beginning of this deceleration is consistent with the fall in the Ca^{2+} transient [3]). This deceleration develops slowly and then more rapidly, as indicated by the slowly increasing intensity of the forward decompression wave. Investigators of an earlier generation might have seen in the time course of this decompression wave a description of the decline of the "active state" [9].

In Fig. 7, the measured pressure and flow waveforms recorded from the descending thoracic aorta are quite different and irregular. Our analysis confirms the generally assumed presence of a reflected, late-systolic compression wave. However, the contours of the respective measured pressure and flow waveforms seem to be largely defined by the effects of an earlier reflected *decompression* wave. (This may be the result of the branching pattern below the

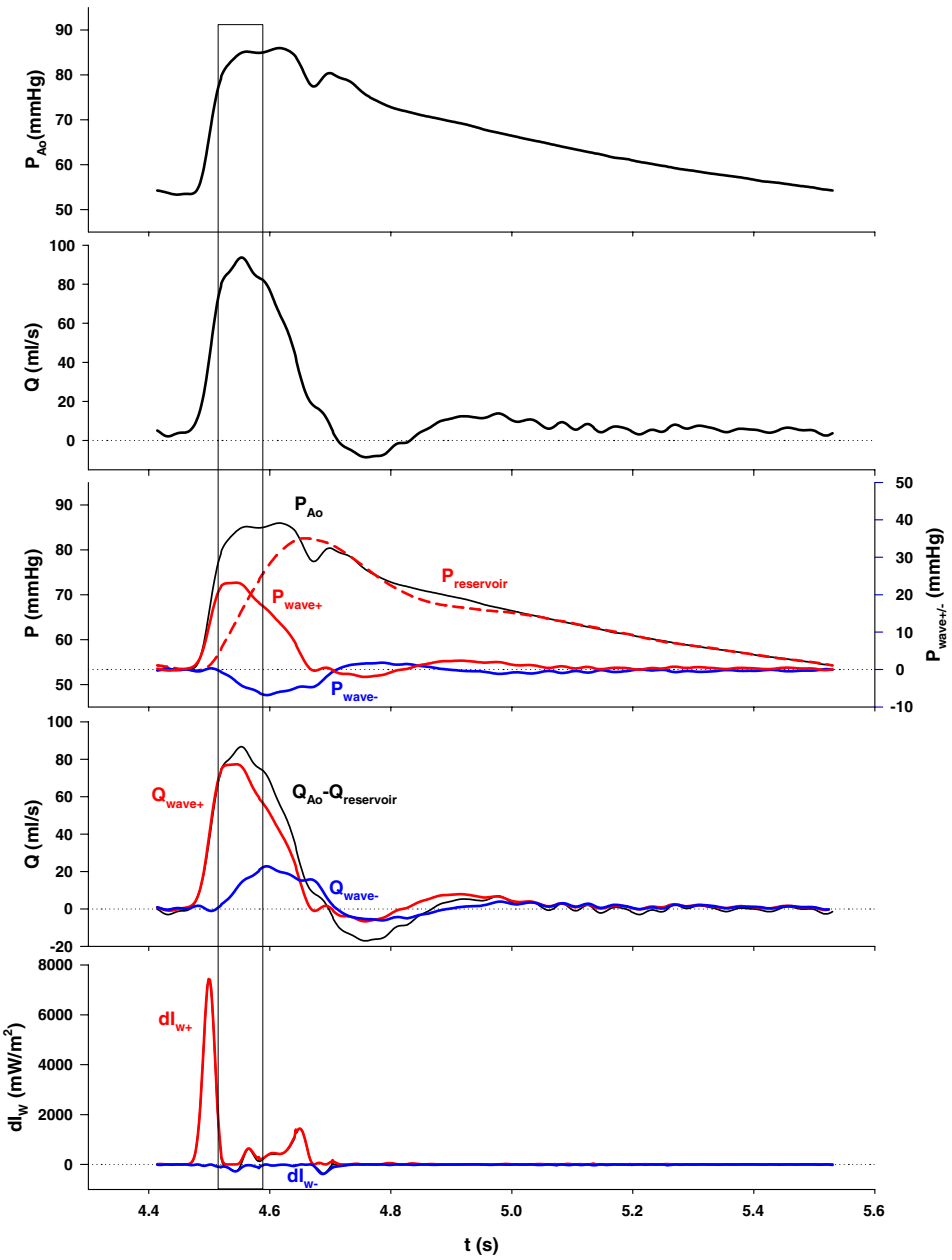

Fig. 7 Reservoir–wave analysis of data recorded from the descending aorta, 20 cm from the aortic root, in a dog. See Fig. 6 for a description of the panels. Note that the systolic plateau in pressure is largely due to an early systolic backward-traveling decompression wave

diaphragm where, over the length of a few centimeters, the descending aorta gives off several large branches; the sum of the effective cross-sections of the daughter vessels may be greater than that of the mother vessel [1, 18]). This decompression wave appears to create a plateau in the pressure waveform and augment the flow waveform.

In both figures, the pressure and flow due to forward- and backward-traveling waves are the respective time-integrals of $dP_{\pm}$ and $dU_{\pm}$. This would seem to be the same as what is done in the impedance approach but the results are entirely different after the reservoir pressure has been subtracted out. The impedance approach generates equal positive and negative "flow waves" during diastole [27]; because our analysis is done on the wave-related pressure, not the measured aortic pressure, no such flow waves are generated.

7 Application of reservoir–wave theory to analysis of human arterial hemodynamics

The reservoir–wave theory has recently been applied to analyze the human pressure waveform [4]. This analysis combines aspects of the Windkessel theory proposed by Frank [8] with the wave theories proposed by Womersley [28] and McDonald [11]. By combining these two models,

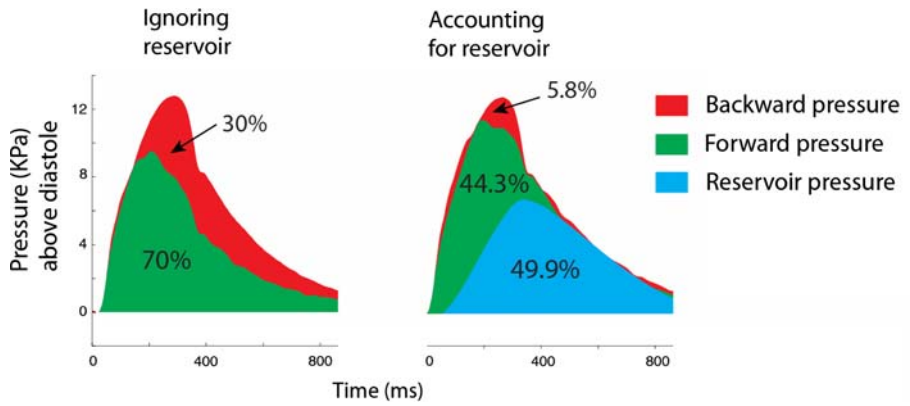

Fig. 8 Simultaneous pressure and flow velocity was recorded in the proximal aorta using intra-arterial wires in a human subject. Pressure was separated into forward- and backward-pressure both ignoring (*left panel*) and accounting for the reservoir pressure (*right panel*). When reservoir pressure was accounted for both backward- and forward-pressure are significantly reduced and reservoir pressure was found to be the largest constituent. These findings suggest that backward-(reflected-) pressure is only a small contributor to overall pressure when the reservoir is accounted for. *Percentages* are representative for the entire data set

the analysis is not subject to the same assumption on which the individual theories are based [28]. In an invasive study to assess the varying contributions of wave reflection and the reservoir to measured pressure, intra-arterial pressure and flow velocity were measured in 19 subjects (mean age 54 years) with sensor-tipped wires in the proximal aorta using a method previously described [5]. Pressure was separated into reservoir and wave pressure [4] and wave pressure was subsequently separated into forward- and backward-pressure using WIA. Wave speed was determined using the single-point technique [5].

Using existing wave-only analysis techniques (Fig. 8, left panel), the peak backward- (or reflected-) pressure was found to account for $\sim$30% of total pressure, and the peak forward-pressure $\sim$70% of total pressure). When the reservoir pressure was accounted for (Fig. 8, right panel) the contribution from reflected waves fell markedly to $\sim$6% of total pressure. The contribution from forward-traveling waves also fell to $\sim$44%. The reservoir component was found to account for the largest rise in peak pressure ($\sim$50% of total pressure). The authors went on to show that while the forward-, backward- and reservoir pressure all increase with age, the increase in backward-pressure is extremely small (2.4 $\pm$ 0.8 mmHg/decade). These findings suggest that the backward- (or reflected-) pressure wave is only a small contributor to overall pressure and as such is unlikely to account for the large changes in pressure augmentation which occur with aging and in disease.

These new findings challenge the widely held wave-reflection mechanism of pressure augmentation [12, 13] which fails to account for the "cushioning" effect of the aortic reservoir, and in doing so is constrained to account for pressure augmentation solely in terms of reflected waves returning from the distal aorta. Using this reservoir–wave model it would be possible to examine the separate effects that different pharmacological agents have on waves and on the reservoir in the human arterial system.

8 Controversial issues

The P_{wave} and Q_{in} are linearly related (see Fig. 2 in Wang et al. [23]). According to our model, P_{wave} is the difference between central P_{aorta} and $P_{reservoir}$ and this suggests that P_{wave} might be considered to represent a gradient and to be the driving pressure for flow (i.e., Q_{in}) from the aortic root into the reservoir. We view this reservoir as an effective, lumped compartment, separated by some distance from the aortic root. The ratio of P_{wave} to Q_{in} has units of resistance and was found to be numerically equal to characteristic impedance, as calculated by Fourier analysis [23]. In the water-hammer equation [10], characteristic impedance is equal to the dP/dQ ratio and, as such, reflects wave behavior as well as any viscous resistance component that might be present. (see "Discussion" pertaining to Figure 5 in Peterson [17]). We suggested that the viscous resistance component was large and that the wave component was minimal [23].

It might be objected that a pressure gradient of $\sim$25 mmHg between the ascending aorta and the aortic reservoir is unreasonably large, given the fact that the difference in mean pressures between the ascending aorta and a small peripheral artery is no more than a tenth of that value. However, we believe that such an objection could arise from a failure to appreciate the difference between peak flow and mean flow. Peak flow is 5–6 times mean flow and, given the non-linear relation between pressure gradient and flow, our interpretation would seem justified.

The conclusion that the viscous resistance component is large and the wave component is minimal is supported by

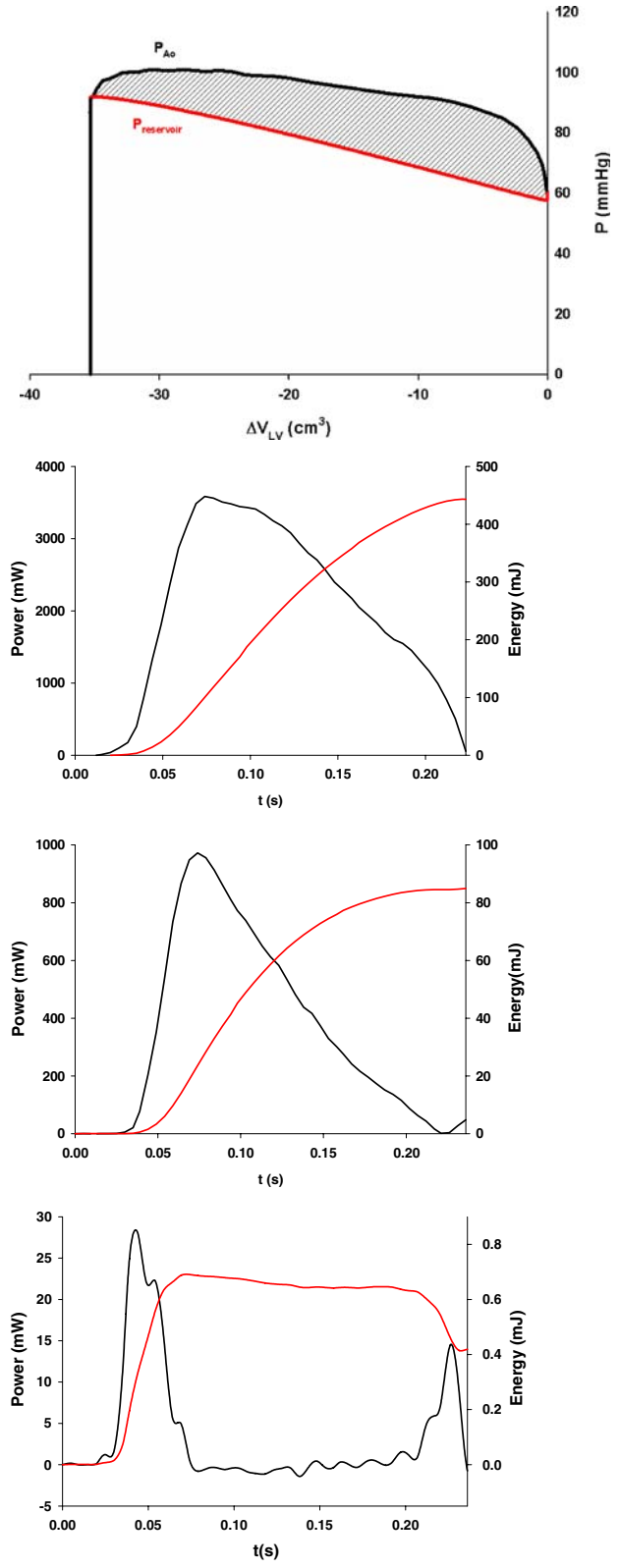

◀ **Fig. 9** The energetics of LV contraction and ejection. At the *top* is an LV *P–V* loop with $P_{reservoir}$ plotted during systole. (This analysis was done on data from an experiment in which LV volume was not measured. Therefore, we used the integrated aortic flow as a measure of LV volume decrease). During the course of ejection, $P_{reservoir}$ (the *red line* in the *top panel*) increases, corresponding to the net increase of aortic reservoir blood volume. The area under this curve represents the increase in potential energy during the expansion of aortic reservoir, an increase that is later expended during diastolic outflow. As P_{wave} is the vertical difference between P_{aorta} (P_{aorta} is assumed to be equal to P_{LV} during systolic ejection) and $P_{reservoir}$, the hatched area in the *top panel* is equal to the integral of $P_{wave} \times Q_{in}$. The *second panel* shows the total *P–V* power (*black*) and work (*red* equal to the area of the *P–V* loop) as a function of time. The *third panel* shows hydraulic power (*black*) and work (*red* the integral of $P_{wave} \times Q_{in}$), which we interpret to be almost entirely a measure of the energy required to pump the blood through the large-artery resistance [17, 24]. The *bottom panel* shows wave intensity (*black* power per unit cross-sectional area) and its time integral (*red* work), which we interpret as the "wave energy" associated with acceleration (the FCW) and deceleration (the FDW) of the stroke volume. In principle, this work is included in the hydraulic work (i.e., the integral of $P_{wave} \times Q_{in}$ in the *panel above*), but it is too small to identify graphically (Color figure online)

the energetic analysis shown in Fig. 9. In the bottom panel, by integrating the area under the wave intensity vs. time curves, we calculated the energy associated with wave-induced acceleration and deceleration and found it to be ~1% of the total hydraulic work (i.e., the integral of the $P_{wave} \times Q_{in}$ product; the third panel), which we interpret to be done in overcoming the proximal resistance [24]. To further evaluate the magnitude of viscous resistance, we recently performed bench-top experiments using plastic tubing with a diameter similar to the canine ascending aorta [21]. We produced quasi-steady flows (~20 L/min) and measured pressure gradients along a horizontal, 1-m length of the tubing, which yielded a value of resistance per length (4.0 mmHg/L per min per m). We then took the value of P_{wave}/Q_{in} (1.38 mmHg/L per min) found by Wang et al. [23] and divided it by 4.0 mmHg/L per min per m to obtain an estimate of the distance between the aortic valve and the reservoir compartment, 34 cm, approximately the distance to the renal arteries in the dog. While this estimate could well be inaccurate by a factor of 2 or more, it is not totally implausible, anatomically, and therefore tends to support the interpretation that the value of P_{wave}/Q_{in} represents the hydraulic resistance of the proximal aorta.

In another paper dealing with the Windkessel/reservoir concept, Wang et al. [24] calculated the energy consumed by pumping blood through each of these series resistors, under control conditions and after administration of a vasodilator (sodium nitroprusside) and a vasoconstrictor (Mtx). Although the energy expended by the large-artery resistance was not large normally, it increased substantially (both absolutely and relatively) with nitroprusside administration, when stroke volume was increased and $P_{reservoir}$ was decreased.

Finally, we have recently shown how increases in large-artery resistance might, in large measure, account for systolic hypertension [21].

Therefore, as unconventional and controversial as our interpretation is, we continue to suggest that this P_{wave}/Q_{in} ratio represents the large-artery resistance between the LV and the reservoir [23]. In the 3-element Windkessel (reservoir) circuit [26], characteristic impedance is represented as a resistor between the input and the filter (i.e., the parallel resistance and capacitance), which is an arrangement entirely consistent with a large-artery resistance. We agree with others that the 3-element Windkessel is a very useful approximate representation of the arterial circulation [21]. However, in marked contrast to previous investigators who have used the impedance approach, we propose that the proximal resistance might be, indeed, a large-artery viscous resistance. We also propose that the pressure against which the 3-element Windkessel empties is P_{∞}, which normally equals 30–40 mmHg—greater than 0 or venous pressure or mean circulatory pressure.

It must be recognized that these alternative, reservoir–wave interpretations are as model-based as those of the impedance approach. We feel that our interpretations are internally consistent and that they suggest new physiologic and, perhaps, medical approaches. However, the interpretations derived from the impedance approach are equally internally consistent and they have been used successfully for many years. As they are two internally consistent, model-based approaches, one cannot be used to disprove the other. It is left to the members of the present and future generations of students to identify their individual preferences, based on utility and on their own internal criteria of scientific acceptability.

9 Conclusions

As illustrated by data recorded from the proximal and distal aorta, from the inferior and superior venae cavae, and from the left heart, WIA yields qualitatively different results when performed after the contribution of volume-related changes in pressure have been accounted for. Further experimental and clinical investigations will be required to evaluate this alternative approach to understanding cardiovascular hemodynamics.

References

1. Alexander RS (1953) The genesis of the aortic standing wave. Circ Res 1:145–151
2. Arts T, Kruger RTI, van Greven W, Lambregts JAC, Reneman RS (1979) Propagation velocity and reflection of pressure waves in the canine coronary artery. Am J Physiol Heart Circ Physiol 237:H469–H474
3. Bers DM (2001) Excitation–contraction coupling and cardiac contractile force. Kluwer Academic Press, Dordrecht
4. Davies JE, Manisty CH, Hadjiloizou N, Aguado-Sierra J, Malik IS, Foale RA, Hughes AD, Mayet J (2008) A unifying explanation of the aortic pressure waveform in humans. J Am Coll Cardiol 49:397A–398A.2007
5. Davies JE, Whinnett ZI, Francis DP, Manisty CH, Aguado-Sierra J, Willson K, Foale RA, Malik IS, Hughes AD, Parker KH, Mayet J (2006) Evidence of a dominant backward-propagating "suction" wave responsible for diastolic coronary filling in humans, attenuated in left ventricular hypertrophy. Circulation 113:1768–1778. doi:10.1161/CIRCULATIONAHA.105.603050
6. Davis MJ, Ferrer PN, Gore RW (1986) Vascular anatomy and hydrostatic pressure profile in the hamster cheek pouch. Am J Physiol 250:H291–H303
7. Flewitt JA, Hobson TN, Wang J Jr, Johnston CR, Shrive NG, Belenkie I, Parker KH, Tyberg JV (2007) Wave intensity analysis of left ventricular filling: application of windkessel theory. Am J Physiol Heart Circ Physiol 292:H2817–H2823. doi:10.1152/ajpheart.00936.2006
8. Frank O (1899) Die Grundform des Arteriellen Pulses. Erste Abhandlung. Mathematische Analyse. Z Biol 37:483–526
9. Khir AW, O'Brien A, Gibbs JSB, Parker KH (2001) Determination of wave speed and wave separation in the arteries. J Biomech 34:1145–1155. doi:10.1016/S0021-9290(01)00076-8
10. Lighthill MJ (1978) Waves in fluids. Cambridge University Press, Cambridge
11. McDonald DA (1955) The relation of pulsatile pressure to flow in arteries. J Physiol 127:533–552
12. Murgo JP, Westerhof N, Giolma JP, Altobelli SA (1980) Aortic input impedance in normal man: relationship to pressure wave forms. Circulation 62:105–116
13. Nichols WW, O'Rourke MF (2005) McDonald's blood flow in arteries. Oxford University Press, New York
14. Parker KH (2008) An introduction to wave intensity analysis. Med Biol Eng Comput
15. Parker KH, Jones CJH (1990) Forward and backward running waves in the arteries: analysis using the method of characteristics. J Biomech Eng 112:322–326. doi:10.1115/1.2891191
16. Parker KH, Jones CJH, Dawson JR, Gibson DG (1988) What stops the flow of blood from the heart? Heart Vessels 4:241–245. doi:10.1007/BF02058593
17. Peterson LH (1954) The dynamics of pulsatile blood flow. Circ Res 2:127–139
18. Remington JW, O'Brien LJ (1970) Construction of aortic flow pulse from pressure pulse. Am J Physiol 218:437–447
19. Sagawa K, Lie RK, Schaefer J (1990) Translation of Otto Frank's paper "Die Grundform des Arteriellen Pulses" Zeitschrift fur Biologie 37:483–526 (1899). J Mol Cell Cardiol 22:253–277. doi:10.1016/0022-2828(90)91459-K
20. Sun Y-H, Anderson TJ, Parker KH, Tyberg JV (2000) Wave-intensity analysis: a new approach to coronary dynamics. J Appl Physiol 89:1636–1644
21. Tyberg JV, Shrive NG, Bouwmeester JC, Parker KH, Wang JJ (2008) The reservoir–wave paradigm: potential implications for hypertension. Curr Hypertens Rep 4:203–212. doi:10.2174/157340208785132572
22. Wang JJ, Flewitt JA, Shrive NG, Parker KH, Tyberg JV (2006) Systemic venous circulation. Waves propagating on a windkessel: relation of arterial and venous windkessels to systemic vascular resistance. Am J Physiol Heart Circ Physiol 290:H154–H162. doi:10.1152/ajpheart.00494.2005
23. Wang JJ, O'Brien AB, Shrive NG, Parker KH, Tyberg JV (2003) Time-domain representation of ventricular–arterial coupling as a windkessel and wave system. Am J Physiol Heart Circ Physiol 284:H1358–H1368
24. Wang JJ, Shrive NG, Parker KH, Tyberg JV (2008) Effects of vasoconstriction and vasodilatation on LV and segmental

circulatory energetics. Am J Physiol Heart Circ Physiol 294:H1216–H1225. doi:10.1152/ajpheart.00983.2007
25. Wang Z, Jalali F, Sun YH, Wang JJ, Parker KH, Tyberg JV (2005) Assessment of left ventricular diastolic suction in dogs using wave-intensity analysis. Am J Physiol Heart Circ Physiol 288:H1641–H1651. doi:10.1152/ajpheart.00181.2004
26. Westerhof N, Elzinga G, Sipkema P (1971) An artificial arterial system for pumping hearts. J Appl Physiol 31:776–781
27. Westerhof N, Sipkema P, van den Bos GC, Elzinga G (1972) Forward and backward waves in the arterial system. Cardiovasc Res 6:648–656. doi:10.1093/cvr/6.6.648
28. Womersley JR (1955) Method for the calculation of velocity, rate of flow and viscous drag in arteries when the pressure gradient is known. J Physiol 127:553–563